University of Malta Engines

Introduction:

Engine simulation has become an integral part of engine development. Although it cannot be used independently from physical experimentation, it can still potentially reduce experimentation time in the sense that the main regions of physical experimentation can be chosen from the full spectrum of experiments.

The three authors presenting this work have modest experience in the field of internal combustion, particularly in the areas of engine simulation, electronic fuel injection implementation, mechanical engine friction and valvetrain design. In this assignment, these areas were combined to provide a holistic approach. It is to be brought to attention that none of the contributors had previous experience with GT-Suite or ModeFRONTIER. In previous work, engine simulation was usually carried out with Ricardo WAVE, which was introduced in MEC4011 *Power Plants* module [1]. This challenged the team to familiarise ourselves with GT-Suite, and convert our previous knowledge on engine simulation to provide the required deliverables, along with some experimental tests carried out at the Thermodynamics Lab of University of Malta. Apart from the preparatory work in previous months the team devoted around 250 hours collectively in the last week before submission.

Air Filter Flow Testing:

Prior to modelling the complete intake system, it was thought to be of an educational value to flow test several air filters and compare their performance. In total, four air filters were flow tested using a centrifugal blower, where the air filter was connected to the suction side of the blower through a 50mm diameter smooth pipe. A properly sized hole along the diameter of the pipe was drilled 500mm (10D) downstream of the air filter and smoothened to suit a pitot static tube traversing the flow. The difference in pressure between the dynamic and static ports of the pitot tube was read from an inclined manometer, from which the peak fluid velocity was found. The blower's rotational speed was varied by a variable frequency drive and the range between 10Hz to 60Hz was covered, which in total resulted in a spectrum between 9.6g/s and 80g/s.

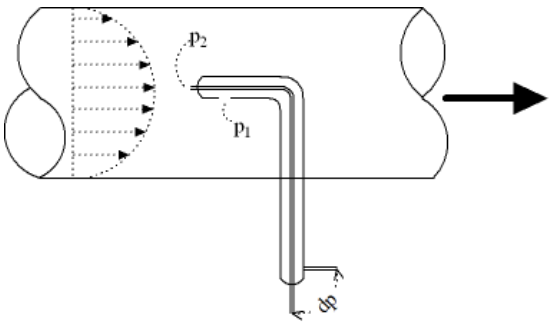

Figure 1: *A graphical representation of flow in pipes, showing the velocity distribution and pitot tube.* **[11]**

It is widely known that for flow in pipes, by the Bernoulli Equation;

$$P_1 + \frac{\rho {v_1}^2}{2} + z_1 \rho g = P_2 + \frac{\rho {v_2}^2}{2} + z_2 \rho g$$

State 1 is taken at an arbitrary point on the centre axis in the fully developed flow, upstream of the pitot tube, whereas state 2 is taken to be the stagnation point. This implies that $v_2 = 0$. Since state 1

and state 2 are on the same elevation, the two potential energy terms cancel out from both sides of the equation, which results in:

$$P_1 + \frac{\rho {v_1}^2}{2} = P_2$$

$$=> \ v_1 = \sqrt{\frac{2(P_2 - P_1)}{\rho}} \qquad \ldots (1)$$

By the 1/7th power law, the average velocity v_{avg} is equal to 0.82 of the peak velocity. [2]

$$\therefore \ v_{avg} = 0.82 v_1$$

Therefore, the volumetric flow rate may be found as:

$$Q\ [m^3/s] = A_{pipe} v_{avg} \qquad \ldots (2)$$

The graph of the volumetric flow rate against the change in pressure across the air filter was plotted in Figure 2 for all the air filters tested.

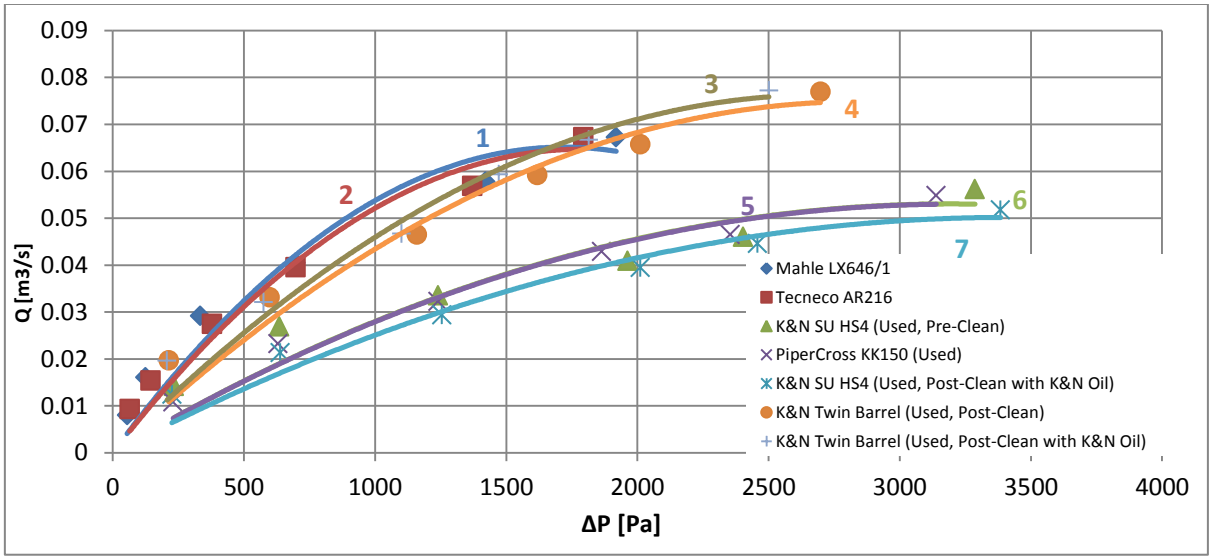

Figure 2: *The graph of Volumetric Flow Rate [m^3/s] against DeltaP [Pa]*

As can be seen from Figure 2, the larger filters, being the Mahle, Tecneco and K&N twin barrel filters showed better flow characteristics than the small K&N SU HS4 and the KK150 filters. Table 1 shows the respective flow areas of each air filter and according to such values, the flow curve of each filter were corrected for a common flow area. The resulting graph is shown in Figure 3.

Table 1: *The respective flow areas of each air filter.*

Air Filter	**Effective Flow Area [cm^2]**	**Normalised Areas [cm^2]**
Mahle LX646/1	362.56	7.71
Tecneco AR216	673.20	14.31
K&N SU HS4	47.04	1.00
PiperCross KK150	20.15	0.43
K&N Twin Barrel	231.04	0.49

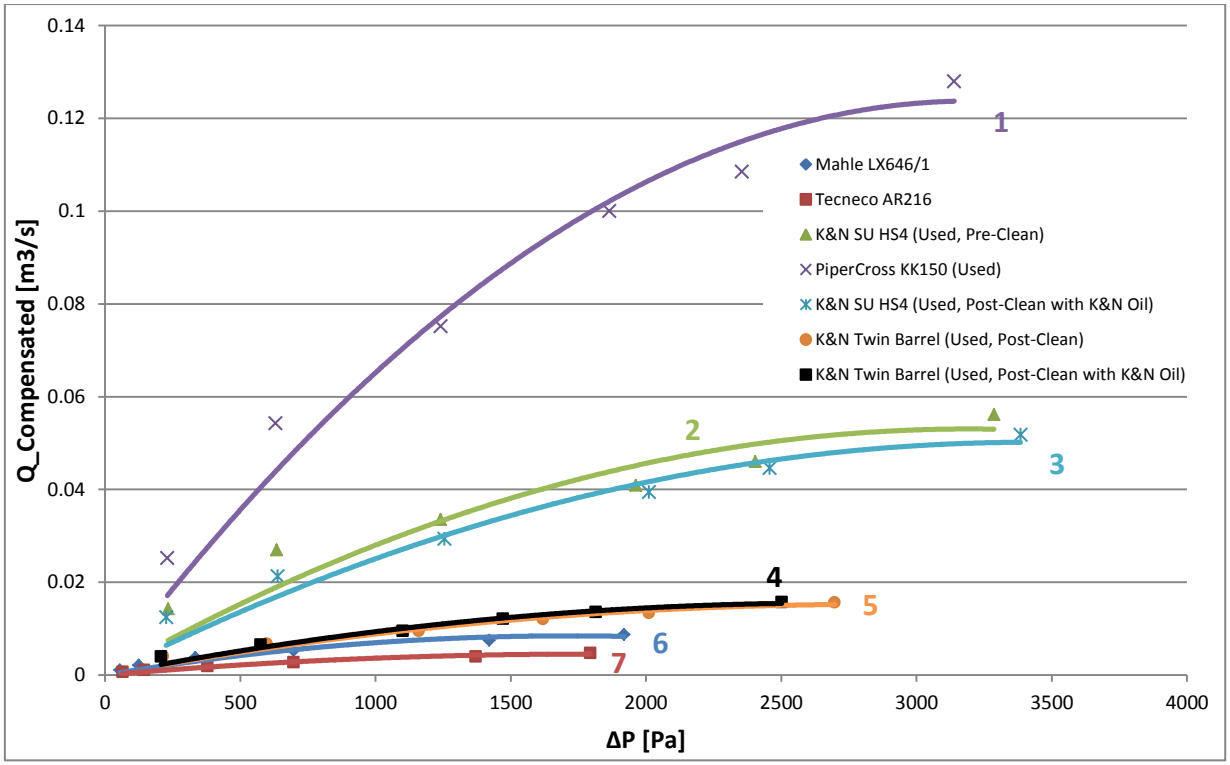

Figure 3: *The graph of compensated volumetric flow rate [m^3/s] against DeltaP [Pa].*

The trendline equations and R-squared values for the filters plotted in Figure 3 are given in Table 1.

Table 2: *The trendline equations for the respective air filters of Figure 3.*

Curve No.	Trendline Equation	R-Squared Value
1	$Q_c = -(1x10^{-8})\Delta P^2 + (8x10^{-5})\Delta P$	0.9663
2	$Q_c = -(5x10^{-9})\Delta P^2 + (3x10^{-5})\Delta P$	0.8608
3	$Q_c = -(4x10^{-9})\Delta P^2 + (3x10^{-5})\Delta P$	0.9400
4	$Q_c = -(2x10^{-9})\Delta P^2 + (1x10^{-5})\Delta P$	0.9608
5	$Q_c = -(2x10^{-9})\Delta P^2 + (1x10^{-5})\Delta P$	0.9458
6	$Q_c = -(3x10^{-9})\Delta P^2 + (1x10^{-5})\Delta P$	0.9462
7	$Q_c = -(1x10^{-9})\Delta P^2 + (5x10^{-5})\Delta P$	0.9674

Normalising the flow curves to a common effective flow area, allows an easy comparison of the filtration material. Evidently, Figure 3 shows that the PiperCross filter has superior flow characteristics (to the detriment of filtration due to large pores) compared to the other filters.

Figure 4: *The air filterflow test setup*

The two K&N filters (SU HS4 and Twin Barrel), believed to have the same filtration material seemed to have significantly different flow characteristics, which may be originating from the shape of the respective filters. The K&N SU HS4 filter performed better before the cleaning treatment. It is in the opinion of the authors that the application of the treatment oil to the filter according to the manufacturer specification has impeded slightly the flow characteristics, which however is deemed to improve the filtration characteristics.

Constructing the Single Cylinder 250cc Model in GTI-ISE 7.5:

To familiarise ourselves with GT-Suite, the "Engine Performance Tutorial" was read and the relevant models were built successfully. As a start point for this work, the "1cylSI-final.gtm" example model was used. To suit the aim of this assignment, several modifications had to be done to the example, the first one being to convert the engine to a 4-valve configuration.

The base intake and exhaust valve lift profiles were obtained from the GT-ISE 7.5 'template.gtm'. It was noted that such valve lift curves had a very small duration with negligible overlap.

Increasing the engine speed reduces the amount of time available for the fresh intake charge to be induced in the cylinder and the exhaust gases to be expelled. To improve considerably the volumetric efficiency of the engine at higher engine speeds, the duration for both valves should be adequately increased.

Increasing the intake valve duration would mean that the valve opens at the end of the exhaust stroke and closes during compression. It is usually desirable to account for the width of the lift curve due to a larger duration by shifting the curve to the exhaust stroke, meaning that the intake valve starts opening at around $52 Deg\ BTDC$. Apart from increasing the time in which the intake charge can be induced, volumetric efficiency also benefits from the effect of the displacement phase of the exhaust stroke.

Similar reasoning was applied to the exhaust valve. If the exhaust valve opens at around $72 Deg\ BBDC$, the incylinder pressure which would still be at a reasonably high value would create a large differential pressure across the exhaust valve and consequently improves to a great extent the scavenging effect through an improved blowdown phase.

To apply this reasoning to our model, the graphs acquired from the 'template.gtm' were modified extensively. The intake lift curve was made to have an initial estimate of 210 Deg duration at 1mm lift, with an anchor at 230Deg from TDC firing. The exhaust valves were made to have an initial duration of 210 Deg at 1mm lift and an anchor at 130 Deg from TDC firing. This meant that the initial valves overlap was of 112 Deg. All the angles given are in crank angle. Both the lift and duration of both the intake and exhaust valves were parameterised with variable names [intdur], [intlift] for the intake valve and [exhdur], [exhlift] for the exhaust valve respectively through a multiplier. Unfortunately, since the number of parameterised variables was quite large, the anchor had to be fixed and thus wasn't optimised. Even though having faced this limitation, the overlap of the intake and exhaust valves was still varied through the variation of the valve durations.

Initially the flow coefficients for the intake and exhaust valves were both imported from the 'template.gtm' however after running the simulation once, it was noticed that an error was shown which said that due to a large ratio of L/D, the computation outrun the curve range. This meant that either the maximum L/D had to be reduced by reducing the maximum lift or increasing the valve diameter or otherwise another flow coefficient curve had to be used. The team opted for the second option, and the flow coefficients used were those reported by Farrugia [3], as obtained on a flow bench test of a Honda F2 600cc engine. When such flow coefficient graphs were compared with

that of the 'template.gtm', both graphs showed similar values, however that acquired by Farrugia [3] had a slightly larger range which allowed the necessary computations.

Constructing the Elements:

After converting the "1cylSI-final.gtm" example to four valves, the two intake valves were connected with a Y-Junction through a small length of pipe. This was also applied for the exhaust side. The two Y-Junctions were in turn connected to a small length of pipe to model the remaining portion of the intake and exhaust ports. Figure 5 shows the elements incorporated.

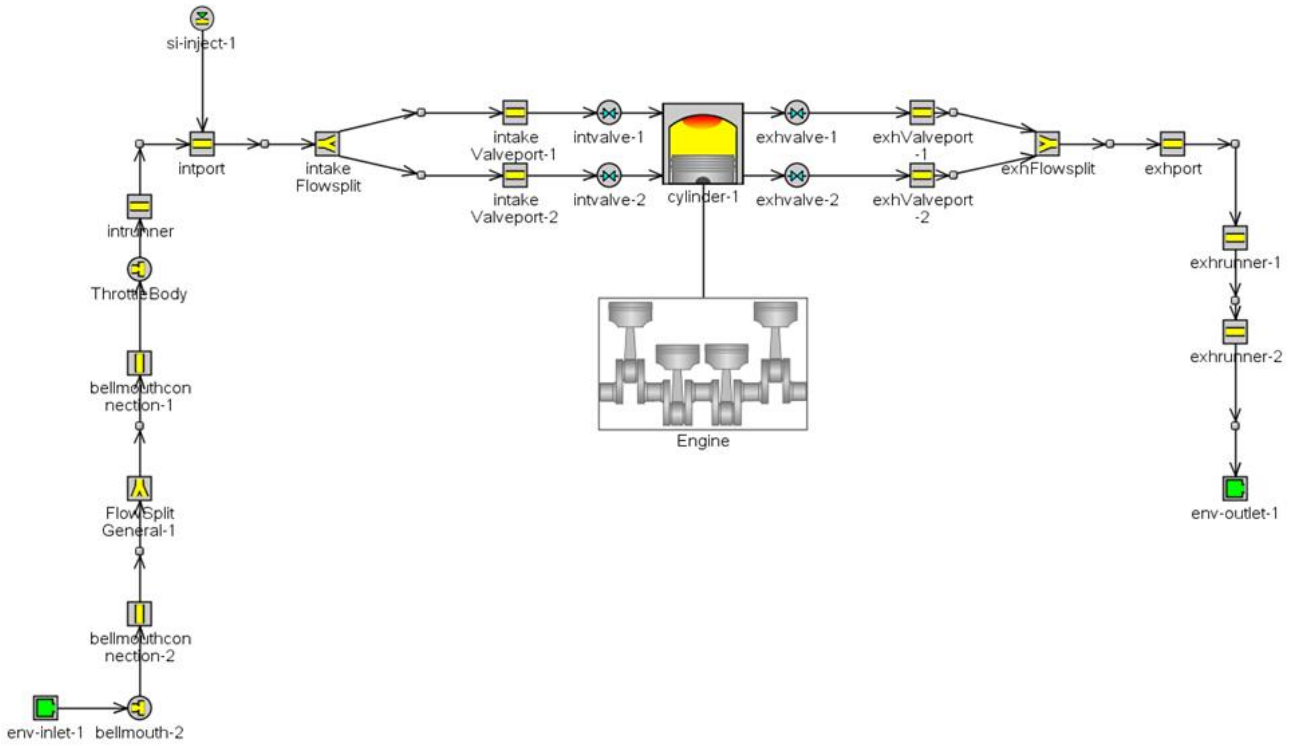

Figure 5: *The model including the ports, runners, valves and throttle.*

On the intake side of the engine, a bellmouth was assigned with a small length of round pipe to introduce the air into the throttle body. The bellmouth was also used as the mass flow sensor element to compute the mass of fuel injected in retaining the AFR constant. It was noted that the default value of 6g/s for the mass flow rate of the injector had to be increased to 10g/s. For the default value of 6g/s, the engine speed ranges higher than 14000RPM were noticed to have an AFR of around 17:1.

The throttle body diameter was parametrised by the variable [D_Throttle]. Downstream of the throttle body, the intake runner was modelled with a round pipe. Both the diameter and the length of the runner were parameterised with variable names [intrunnerdiameter] and [intrunnerlength]. The small piece of round pipe between the bellmouth and the throttle body was fixed with a diameter of 52mm and a length of 60mm. Since the engine was to be operated up to speeds of 17500RPM, the intake lengths were initially kept short with a generous diameter. The length of the round pipe between the bellmouth and the throttle was however not parametrised due to limit on computational power.

With regards to Thermal and Pressure Drop considerations on the intake system, the wall temperatures of the bellmouth connection and the intake runner were both assigned as 300K due to

the fact that they are in constant contact with cool intake air. The surface roughness of both the bellmouth connection and the intake runner were considered to be similar to smooth plastic.

The intake port elements were all deemed to be frictionless (as stated by Farrugia [3] due to the fact that the flow bench tests C_d also incorporates the wall friction) with wall temperatures of 373K. This particular temperature was chosen to symbolise the cylinder head temperature, with which the intake air comes in contact in the intake port. The two pipes closest to the intake valves were both parametrised on the length with variable [intvalveportlength]. The diameter of these two pipes was made equal to the valve diameter which was parameterised with a variable name [D_ASP]. The single round pipe connecting to the intake Y-junction was also parameterised on its length and diameter with variable names [intportlength] and [intportdiameter] respectevely. The flow split general element was assigned with a constant volume of $31808mm^3$and a default constant surface area.

For the first initial runs, the airbox volume was not modelled. However after familiarising ourselves with the software and the aircleaner flow tests were conducted, the model was modified to include the airbox. Furthermore a Co-Simulation using GT-Suite and Fluent was also done and explained in detail later in the text.

The exhaust side of the engine was modelled with two simple lengths of round pipe; one of which modelled the exhaust runner, and one modelled a small piece of exhaust pipe. The pipe modelling the exhaust runner was parametrised on the length and diameter with variable names [exhrunlength] and [exhrundiameter] whereas the small piece of exhaust pipe was modelled with a fixed length of 200mm and a diameter equal to that of the exhaust runner.

The exhaust duct in head was modelled as a Y-Junction connected through two small lengths of round pipe to the valve. Downstream of the Y-Junction, a round pipe element was assigned which model the remaining length of the exhaust port. The length and diameters of the two similar pipes were assigned with the same parametrised diameter, having a variable name of [D_SCA]. The same pipes were also optimised on their length with variable name [exhvalveportlength]. The other pipe connected to the Y-Junction was parametrised on both the length and diameter with variable names of [exhportlength] and [exhportdiameter] respectively.

The thermal aspect of the exhaust duct in head was modelled with a temperature of 373K which represents the cylinder head temperature, with which the exhaust comes in contact. The roughness of the same port was assigned to be frictionless.

The intake runner was assigned with a roughness similar to that of cast iron with a wall temperature computed from the 'WallTempSolver' sub model, factoring cylindrical geometry, material properties, external temperature, radiation and convection. The external convection coefficient was taken to be $15W/m^2K$. The external convection temperature and radiation sink were both considered to be 323K which represents the exhaust environment temperature.

Compression Ratio:

The compression ratio used in this model was fixed to 12:1, which is a reasonable value for a motorcycle engine. The possibility of increasing the compression ratio to the maximum allowed by the specifications was discussed, however it was agreed that going beyond the 12:1 limit would create a problem with the fuel chosen. For this model the standard GT Suite Fuel (Indolene) was used which has a RON rating of 98 [4], whereas commercially available fuel usually has a RON rating of 95.

For the compression ratio to be optimised it would be ideal to include a knock model in the simulation and the compression ratio can be increased to a suitable safe limit which prohibit autoignition.

From experiments done by Azzopardi [5] on a 600cc Kawasaki ZX6r engine, the knock magnitude was investigated from incylinder pressure measurements and compared to feedbacks from commercial knock sensors. The frequencies of knock were also investigated through computations of the Fast Fourier Transform. Due to the AVL ZL21 sideways oriented pressure sensing diaphragm, only the first mode of knock could be captured. Another section of this study regarded the calibration of the commercially available knock sensor with the data acquired from the incylinder pressure measurments. The commercially available sensor was then connected to the ZX6r programmable Reata engine management.

From previous work by Grech [6] on 1D engine simulation it was noticed that knock models are not reliable in capturing knock, and furthermore require intense computational power. Thus for the scope of this assignment the compression ratio could not be decided based on knock study and hence a conservative value of 12:1 was implemented.

Design of Experiment:

One of the fundamental learning experiences of this work regarded the Design of Experiments (DOE) and the respective optimisations. After the complete model was built, the parametrised geometries described in the previous section were to be optimised.

In total nineteen parametrised variables were assigned. This made it computationally impossible to run the experiments in one batch, thus these were split up over two batches with the intake experiments and optimisations done separately and independently of the exhaust side. According to Sammut [7], the optimisations on the intake can be run separately from the exhaust. This was also confirmed from a simple model which the authors ran on the same single cylinder engine with the intake and exhaust optimisations run at once but for a very small engine speed range and limited number of parameters. The interactions obtained from this run are plot in Figure 6.

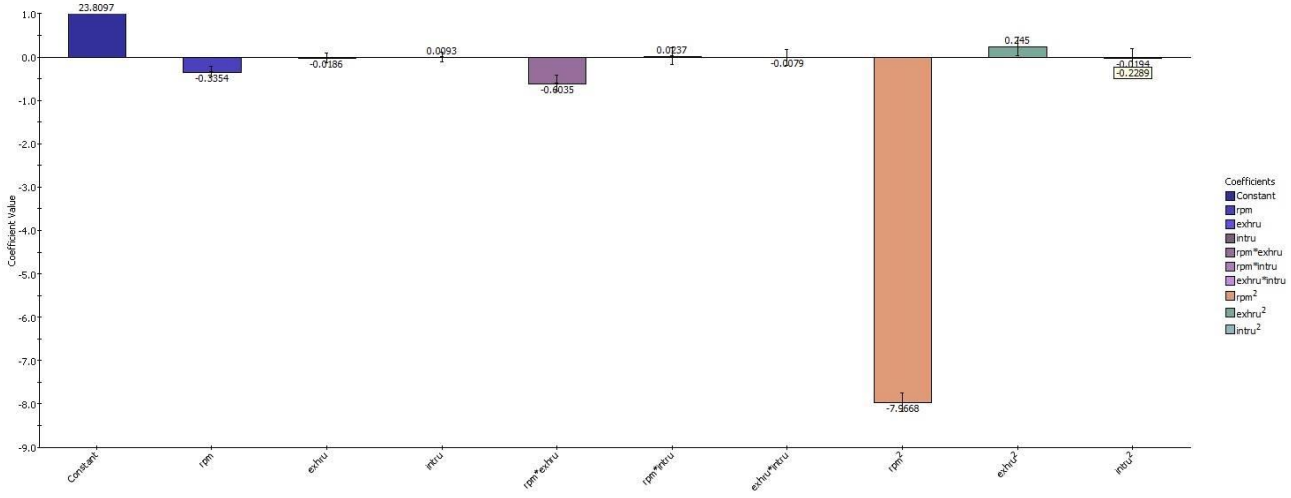

Figure 6: *The interactions of the intake and exhaust showing negligible effect on the torque and power.*

As can be seen from the above figure, the interaction effect of intake runner and the exhaust runner as obtained from the variables [intrun] and [exhrun] are minimal.

The Design of Experiment type was chosen to be the Full Factorial. This type assigns all number of permutations required by the number of variables assigned as experiment parameters. The range of variation of each parameter was determined by assigning the minimum and maximum values, and each range should then be split into the desired number of levels. The number of levels determines the number of experiments that would be carried out in the Full Factorial type of DOE.

After splitting up the intake and exhaust DOE's it was still noticed that the total number of experiments exceeded the ten thousand which requires distributed simulation. Thus to keep the number of experiments below the ten thousand mark the number of levels was set was quite a rough value which unfortunately reduced the resolution of the model. Two different strategies to overcome this limitation were thought of. The first is to run the detailed fine levelled experiments on a very short Engine Speed range with just two levels of engine speed. This would then maximise the torque by optimising all the parametrised variables for the two levels of engine speed. By doing the same procedure for the global range of engine speed in steps of two would then result in a set of optimised parameters for each level of engine speed. This would attain a high resolution of the variables to be parametrised without exhausting the available computational resources.

The other simpler strategy which was used for this assignment due to time restrictions was to run a model with different cases to obtain a general torque curve with engine speed. From this graph, the salient points which represent the region of operation of the engine was chosen and the DOE was then run only on this region of interest of engine speed with only five levels. Such method decreased the number of experiments to an acceptable level, however limited both the range and resolution of the model. Figure 7 shown below shows the general non-optimised torque curve.

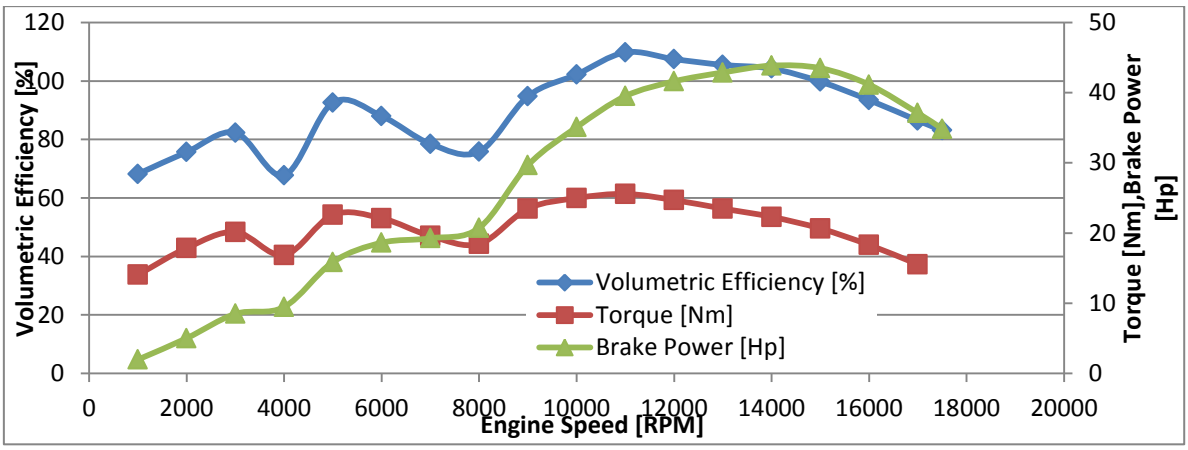

Figure 7: *The graph of volumetric efficiency, brake power and torque with engine speed.*

As can be seen, a torque dip is seen at the range of engine speeds between 7000RPM and 9000RPM, whereas a peak torque of 25Nm was seen at 11000RPM. Beyond this region, the torque falls to around 15Nm. Since the engine was designed to rev up to 17500RPM, speeds below the 5000RPM mark were seen to be superfluous for the particular engine. Thus the range of optimisation was chosen to be between 5000RPM and 17500RPM. The five levels of optimisation were stratified by the 5000RPM, 8125RPM, 11250RPM, 14375RPM and 17500RPM.

In order to assess power curves with good judgement the drop in engine speed for each gear shift from 17,000rpm was found. Gear ratios for a racing motorcycle, namely a Honda CBR250RR were found. The ratios were as follows: 2.733, 2.000, 1.590, 1.333, 1.153, 1.035 and typical ratios for primary reduction, final reduction and wheel size were used. This resulted in a calculated from 17000 to approximately 12000 rpm between 1st and 2nd gear. It is noted that this drop is the biggest

drop as the drops in other up shifts result in progressively smaller drops in RPM. The range of engine speeds found was covered by the five levels of optimisation.

The first run of experiments was for the intake side of the engine. Table 3 below shows the range of variation for each variable and the number of levels. The total number of experiments done was 2560. The R-square value for the curve fitting was found to be 0.68.

Table 3: *The parametrised variables, their ranges and levels for the intake side {DOE_intake_no1}*

Parametrized Variable	Minimum	Maximum	No. of Levels
Engine Speed	5000	17500	5
D_ASP	33	35	2
D_Throttle	49	52	2
intDur	1	1.2	2
intLift	1	1.1	2
Intportdiameter	38	41	2
Intportlength	13	17	2
Intrunnerdiameter	49	52	2
intrunnerlength	60	80	2
intvalveportlength	12	14	2
No. of Experiments			2560

The Second run of experiments regarded that of the exhaust. The parametrised variables together with their ranges and number of levels are shown in Table 4. The number of experiments performed was 9720. Since the number of experiments by the Full Factorial reached high values, the compilation of experiments took three hours and twenty minutes to complete. Due to the memory limitation the curve fitting of the experiments had to be split into two by the engine speed categories. The R-squared values of the two fits were 0.94 and 0.9992. This is explained in detail further on.

Table 4: *The parametrised variables, their ranges and levels for the exhaust side {DOE_exhaust_no1}*

Parametrized Variable	Minimum	Maximum	No. of Levels
Engine Speed	5000	17500	5
D_SCA	26	27	2
Exhdur	1	1.2	3
Exhmult	0.9	1.1	2
Exhportdiameter	43	46	3
Exhportlength	20	30	3
Exhrundiameter	44	46	2
exhrunlength	180	220	3
exhvalveportlength	22	27	3
No. of Experiments			9720

Optimisation:

After having run the design of experiments in GT-ISE, the torque was maximised for each engine speed and the optimum parameters for obtaining the best torque at each engine speed were consequently found. Different engine speed ranges require different optimum parameters. This imposes a physical limitation on engine design, for example to vary the duration of valves, variable valve timing would be required, similarly intake runner lengths can also be varied to cater for different engine speeds. The optimum parameters at each engine speed are given in Table 5 and Table 6.

Table 5: *The optimum parameters for {DOE_intake_no1} at each engine speed [RPM]*						
RPM	INTDUR	INTLIFT	INTPORTDIA	INTPORTLENGTH	INTRUNDIA	INTRUNLENGTH
5000.0	1.0	1.0	38.1	13.0	49.2	76.8
8125.0	1.0	1.1	38.0	13.0	49.6	79.4
11250.0	1.0	1.1	38.0	13.0	51.0	79.4
14375.0	1.2	1.1	38.0	15.0	49.0	80.0
17500.0	1.2	1.1	38.0	13.0	49.0	80.0

Table 6: *The optimum parameters for {DOE_intake_no1} at each engine speed [RPM]*						
RPM	D_ASP	D_THROTT	RPM	INTVALVEPORTLENGTH	TORQUE	BHP
5000.0	33.1	50.9	5000.0	12.0	22.9	15.2
8125.0	35.0	49.1	8125.0	12.0	24.8	30.0
11250.0	34.7	52.0	11250.0	13.7	24.8	36.1
14375.0	35.0	49.4	14375.0	13.0	21.6	43.2
17500.0	35.0	52.0	17500.0	13.0	17.1	41.6

To simplify matters, a compromise was reached between the optimum values of each engine speed. These carefully-chosen parameters were then assigned as constants to the model and the latter was run with cases of engine speed at 500RPM intervals. The torque curve with the optimum parameters from the DOE and the torque curve with carefully-chosen parameters were plot as curve 1 and curve 3 respectively in Figure 8. As can be seen from the graph, curve 1 which is supposed to have optimum torque for each engine speed seemed to be considerably different as compared to curve 3. It is observed that the curve which was supposed to give the optimum torque at all engine speeds, ie. curve 1, developed 4bhp less than the curve 3, which if anything is expected to be less than optimum due to the compromises required in the selection process. This observation was not well understood.

In curve 3 which shows the plot for the carefully-chosen parameters it was noticed that there was a flat portion between the 6000RPM and the 8000RPM. Furthermore, the torque beyond the 9500RPM seemed to drop abruptly. To try and improve in general the power curve, the duration of the intake valve was increased by a factor of 1.1 and 1.2 consecutively, with the curves being 4 and 5 respectively. It was however noticed that increasing the intake duration worsened the torque distribution over the speed range between 6000RPM and 9000RPM.

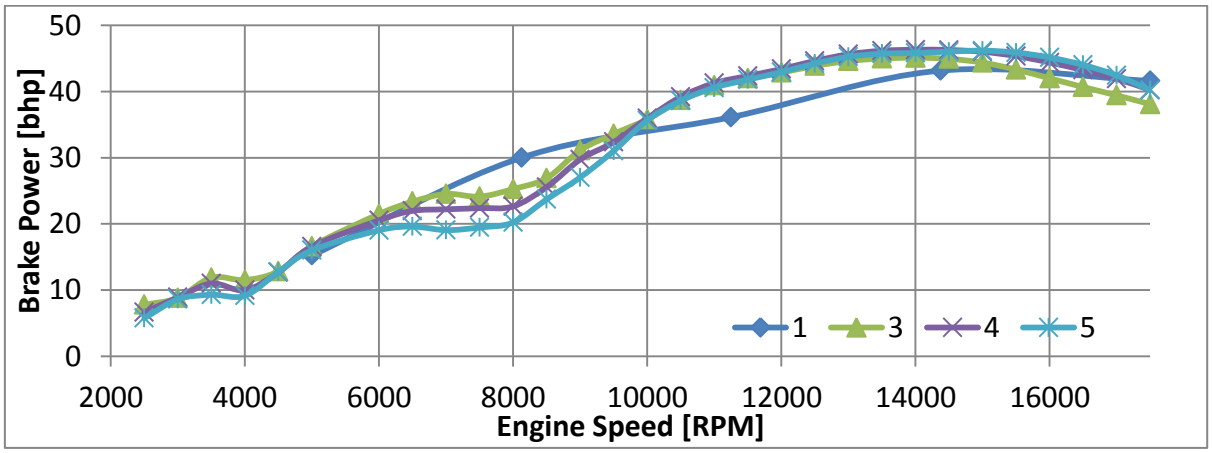

Figure 8: *The graph of power against engine speed for the optimised intake system {DOE_intake_no1}.*

Retaining the intake duration with the 1.2 factor, the intake runner length was varied by 30mm from a minimum of 60mm to a maximum of 90mm. In Figure 9, the plot corresponding to the run with 60mm intake runner length is plot 6 and the one corresponding to 90mm runner length is plot 7. To aid high engine speed regions, it is usually advisable to reduce the length of the port and increase the diameter, however from such plots when the intake runner length was decreased from 90mm to 60mm, a noticeable decrease in power was observed from around 6000RPM all the way to the 17500RPM. Since the curve of the 90mm runner length seemed to develop slightly higher power, the intake runner length was chosen to be 80mm to strike a balance between the two extremities while still giving priority to the longest runner. Curve 7 shows a pronounced dip at the 7500RPM. To try and improve this dip together with reducing the negative gradient at the 17000RPM, the exhaust runner was shortened from the constant value of 400mm as run in the DOE experiment to 300mm. The torque curve of the 80mm intake runner length together with the 300mm exhaust runner are shown in curve 8. As can be seen from the plot, curve 8 shows a significant improvement over the previous case 7. The dip at around the 8000RPM was straightened, whilst the negative gradient at the 7000RPM range was decreased to a great extent. To try and improve slightly more on this condition, the 300mm exhaust runner was reduced to just 200mm and the power curve for this case was plot in curve 9. This plot showed a slight improvement at the 8500RPM region, however it also showed a significant decline in power at the 11000RPM.

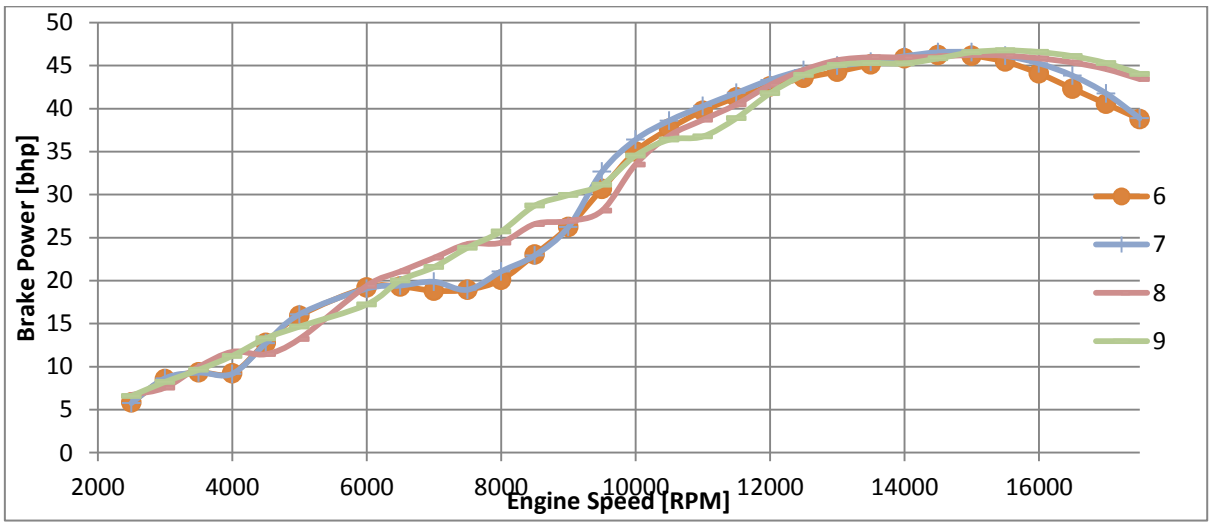

Figure 9: *The graph of power against engine speed for the optimised intake system {DOE_intake_no1} - Continued.*

After optimizing the intake side of the engine, the same procedure was implemented on to the exhaust side. The DOE model was run and the optimum values were chosen for each engine speed range. It must be noted that for such DOE, the number of experiments by the Full Factorial reached the 9700 mark. This large number of experiments created some issues with the fitting of the model surface. The reason was that GT-Power was only using a small portion of the computer's RAM (irrespective of using a 4Gb,8Gb or 32Gb RAM computer), and thus it was reported that insufficient memory was detected. To overcome this limitation, the engine speed range was split into two overlapping sections for the post-processing of the DOE experiment. As can be seen in Figure 10, plots 1 and 2 seem to overlap at the 11500RPM with a shift of 1.15BHP. It was also observed that there was a slight change in gradient at the overlap.

The optimum parameters found for the intake were not inserted in the DOE for the exhaust side, for the simple reason that both DOE's were run at the same time. However the data for the intake side was processed before that of the exhaust side, and thus for the exhaust side, after the carefully-chosen values were chosen from the DOE optimum values, the model was rerun with cases at every

500RPM interval. For such run, the optimum values obtained from the intake model were input to the exhaust cases. This in fact shows in the improvement beyond the 12000RPM range and at the 8000RPM region.

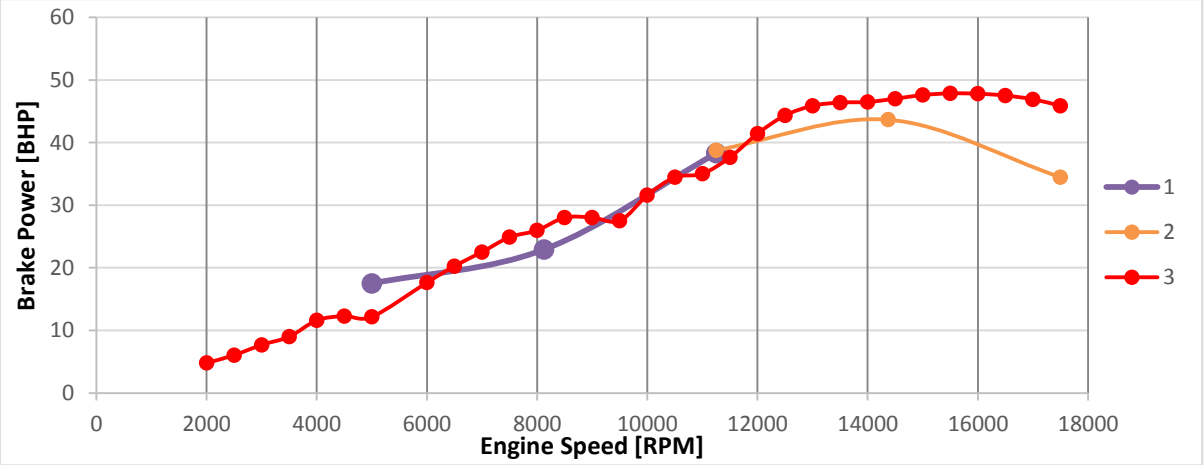

Figure 10: *The graph of Brake Power against Engine Speed for the design of experiment {DOE_exhaust_no1}*

A point which should be mentioned is that the DOE for the intake system described previously was run on a model on which the airbox was not modelled. To capture the effect of the air box whilst monitoring its effect on the already optimised intake parameters, another DOE was run for the intake side, with the airbox modelled as a flow split general. The parametrised variables in this DOE were listed in Table 7 with a total of 7680 experiments. Since the experiment number was also large, the surface fitting had to be split into two, with R-squared values of 0.67 and 0.997.

Table 7: *The parametrised variables, their ranges and levels for the exhaust side {DOE_intake_no2}*

Parametrized Variable	Minimum	Maximum	No. of Levels
Engine Speed	5000	17500	5
D_ASP	33	35	2
D_Throttle	49	52	2
Intdur	1	1.2	3
Intlift	1	1.1	2
intportdiameter	38	41	2
Intportlength	13	17	2
Intrunnerdiameter	49	52	2
intrunnerlength	60	80	2
Intvalveportlength	12	14	2
aboxvolume	0.5e6	1.2e6	2
No. of Experiments			7680

After running the DOE experiment, the best power curves were each plot as obtained from the optimum parameters at each engine speed. This is seen in curves 1A and 1B in Figure 11. Similarly to what was done for the previous DOE's, from the DOE optimum values, a set of carefully-chosen values were found and imposed as constants on the model and the latter was run with several cases on engine speed. Curve 2 shows the graph for these carefully-chosen values. The variation between curves 1A and 1B as compared to curve 2 occurs from the fact that for curve 2, the optimum exhaust parameters as found from the previous DOE were input.

To investigate the effect of the airbox volume, the optimum value found of 1.2Litres was varied to both 0.5L and 2.2L. The curves for the 2.2L, 0.5L and 1.2L airbox are shown in Figure 11 and Figure 12 as plot 4, 5 and 6 respectively.

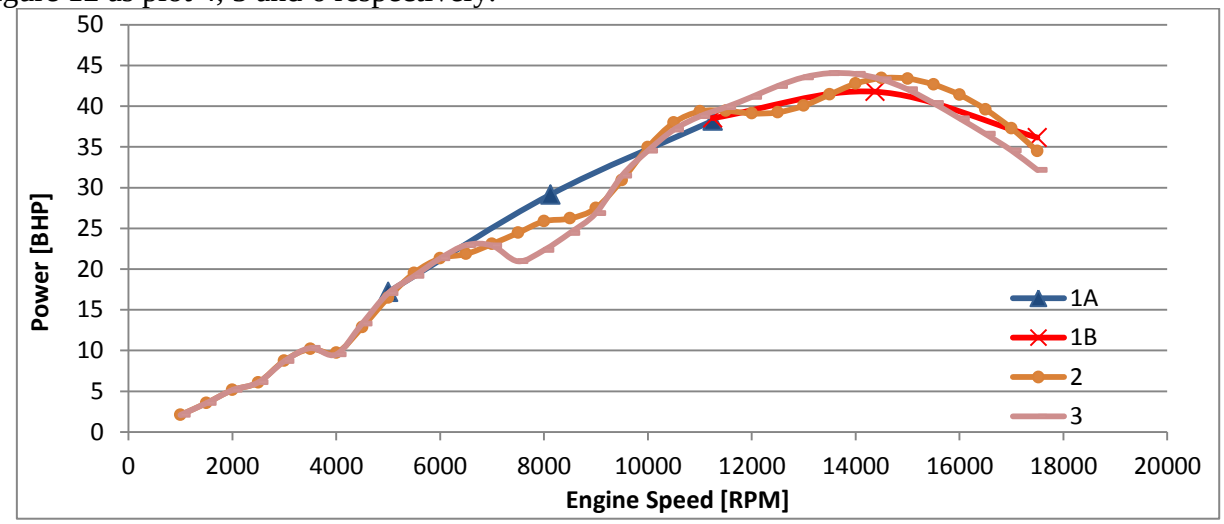

Figure 11: *The graph of Brake Power against Engine Speed for the design of experiment {DOE_intake_no2}*

To understand the concept of the expansion diameter, the model was run with an airbox volume of 1.2L, but with a reduced expansion diameter from 170mm to 100mm. The resulting curve is seen in plot 6, which is very similar to plot 5, the one for the 1.2L volume and 170mm expansion diameter.

Another run was done with to compare the exact same model with no airbox. The resulting curve was plot in 9. As can be seen, the airbox was responsible for a pronounced drop in power over the entire range between 8500RPM and 14500RPM.

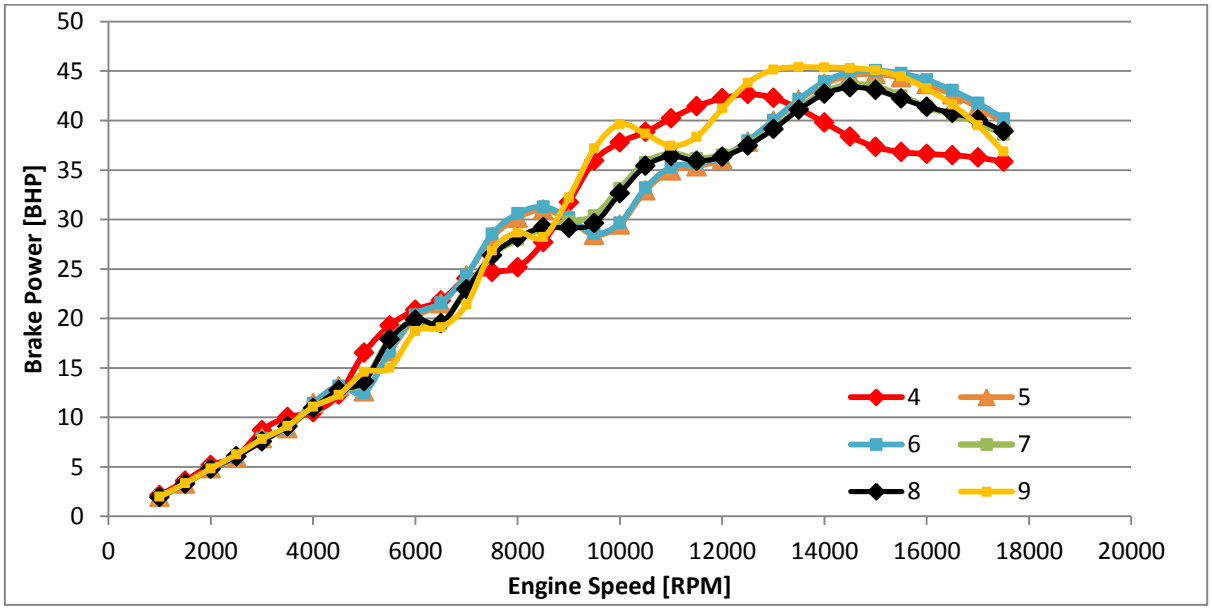

Figure 12: *The graph of Brake Power against Engine Speed for the design of experiment {DOE_intake_no2} - Continued*

To smoothen the crests and troughs seen between the 7000RPM and the 12000RPM on curves 5 and 6, the exhaust runner lengths were reduced from the optimum values previously found in *{DOE_exhaust_no1}* of 300mm to 150mm. The resulting curve was plot in 7. This showed a significant improvement in averaging the crests and troughs found at the discussed regions. Another

run with the exhaust runner equal to 100mm was conducted, however as seen by comparison between curves 7 and 8, no significant difference was seen.

Friction Coefficient Estimation:

Engine friction is one of the variables responsible in reducing engine performance. Friction manifests itself on a significant scale in certain areas of engine operation. It is reported by Singh [8] that engine friction consumes as much as 10% of the power output of the engine at full load, to 100% of the power output at no load. The Stribeck diagram is one of the tools that can be used to identify the nature of the friction, depending on the operating regime of the particular component. The Stribeck diagram plots the coefficient of friction against a dimensionless parameter being a function of mean velocity and load.

The two extremes of operation are boundary friction and hydrodynamic friction. Boundary friction refers to a direct metal-to-metal contact between two respective components. On the other hand hydrodynamic lubrication refers to the instant when two surfaces are completely isolated by a layer of circulating oil. Reducing the engine load and increasing engine speed shifts the operation to hydrodynamic.

To validate the friction estimated from the one dimension engine model, a friction model reported by Singh [8] was applied on the major engine components to find their individual FMEP. The total mean effective pressures were then summated to give the total FMEP as a variable with engine speed. The resulting relationship of TFMEP with engine speed was then compared with that obtained from the engine simulation. Both traces were superimposed on Figure 13.

The one dimensional model was based on the Chen-Flynn correlation where the latter is described by four terms to capture the effect of friction as dependent on several factors of operation. The constant term captures the effect of accessory friction. The second term which varies linearly with piston velocity captures the effect of hydrodynamic friction. Another term takes into consideration the gas loading as represented by the peak combustion pressure. The last term varies in quadratic manner and captures the effect of windage losses in the engine as a function of piston velocity [9].

The empirical friction correlations used were obtained by Singh [8]. It was argued that correlations obtained by authors in the past were obtained from large industrial engines and such correlations were thus inaccurate to predict friction on small scale engines. His interest was in particular in small air cooled SI engines. Considering that the engine under consideration in this assignment is similar to that considered by Singh [8], the empirical correlations reported in his work were used.

When considering friction, it should be explicitly stated which portion of friction is being considered. Rubbing friction is the area of concern in this particular writeup. Rubbing friction refers to the components of friction originating due to contact between two relative moving surfaces and it can be further categorised by the main engine components. The main components under consideration are:

1. Crankshaft Friction
2. Accessory Friction
3. Valvetrain Friction
4. Piston Assembly Friction

Crankshaft friction in particular originates from the interaction of the crank bearings with their respective sleeve bearing. Bearings normally operate in the hydrodynamic region. This induces a form of friction known as ‘turbulent dissipation’ which consists of energy lost in the process of the

pressurisation of the lubricant through the bearing orifices. The relationship used by Singh to calculate crankshaft friction is:

$$\text{FMEP(kPa)}=\left(1.22\times10^{5}\left(\frac{D_b}{B^2Sn_c}\right)\right)_{BST}+\left(3.03\times10^{4}\frac{ND_b^3L_bn_b}{B^2Sn_c}\right)_{MBHT}+\left(1.35\times10^{-10}\left(\frac{D_b^2N^2n_b}{n_c}\right)\right)_{TDT}$$

The next category of rubbing friction is Accessory Friction. Such component is usually regarded as varying in a linear proportion with engine speed, or otherwise it may also be taken as a constant. Accessory friction refers to the power dissipated in ancillary components required in the operation of an engine, such as; oil pump, water pump, alternator, fan drive and much more. Such forces are reported to account up to 20% of the TFMEP according to Singh [8].

$$\text{FMEP(kPa)}=5.06+\left(0.00000145\times N^2\right)$$

Valvetrain friction is another major source of friction. Several valvetrain configurations have their associated friction distribution. It was reported by Heywood [10] that the overhead camshaft configuration is the most efficient in terms of friction. The valvetrain system has two major friction components; the spring force which increases the normal reaction, and the inertial forces. The friction contribution coming from the spring force is significant at low engine speeds, whereas inertial friction contribution is significant at higher engine speeds. The empirical relationship used by Singh is given in the below equation.

$$\text{FMEP(kPa)}=\left(244\frac{Nn_b}{B^2Sn_c}\right)_{MBHT}+\left(1.81\times10^{-2}\left(1+\frac{1000}{N}\right)\frac{kL_vn_v}{V_d}\right)_{FFT}+\left(0.5\frac{L_v^{1.5}N^{0.5}n_v}{BSn_c}\right)_{OHLT}+\left(\left(1+\frac{1000}{N}\right)\frac{kL_v^2n_v}{V_d}\right)_{OMLT}$$

Reciprocating friction refers to the component of rubbing friction which originates mainly from the piston motion. The reciprocating piston has a complex transition between the hydrodynamic friction and the boundary friction. Piston assemblies are usually modelled through four main forces; the gas loading, the force transmitted through the connecting rod, the side thrust loading and the bore frictional force. Near the bottom and top dead centres, since the velocity of the piston slows down to a minimum the friction exhibited is of the boundary type, especially in the vicinity of TDC firing, where apart from the low velocities experienced, the gas loading and high temperatures limit the flow of lubrication between the contacting surfaces and thus boundary friction is promoted.

$$\text{FMEP(kPa)}=\left(294\left(\frac{S_pL_s}{B^2}\right)\right)_{PST}+\left(4.06\times10^{4}\left(1+\frac{1000}{N}\right)\frac{1}{B^2}\right)_{PRFT}+\left(3.03\times10^{4}\frac{ND_b^3L_bn_b}{B^2Sn_c}\right)_{HJBT}+\left(6.89\frac{P_i}{P_a}\left[0.088r_c+0.182r_c^{(1.33-KS_p)}\right]\right)_{GPLT}$$

An Excel file with all the variables in the above equations was done and each of the friction components was computed. The TFMEP graph obtained from Singh's [8] work was then compared to the curve obtained from GT-Power, as computed by Chen-Flynn's correlation. The two graphs can be seen in Figure 13. It should be noted that when Singh's correlation with all its components was used, a very high FMEP resulted. For Singh's correlation to compare to the Chenn Flynn correlation, the geometrical variables assigned for Singh's correlation are those given in Table 8.

Furthermore, for Singh's correlation, the accessory power was assigned a constant of 0.35Bar. Thi is also shown in Figure 13 instead of using the accessory friction given by Singh, a constant of 0.35Bar was added to the other friction components

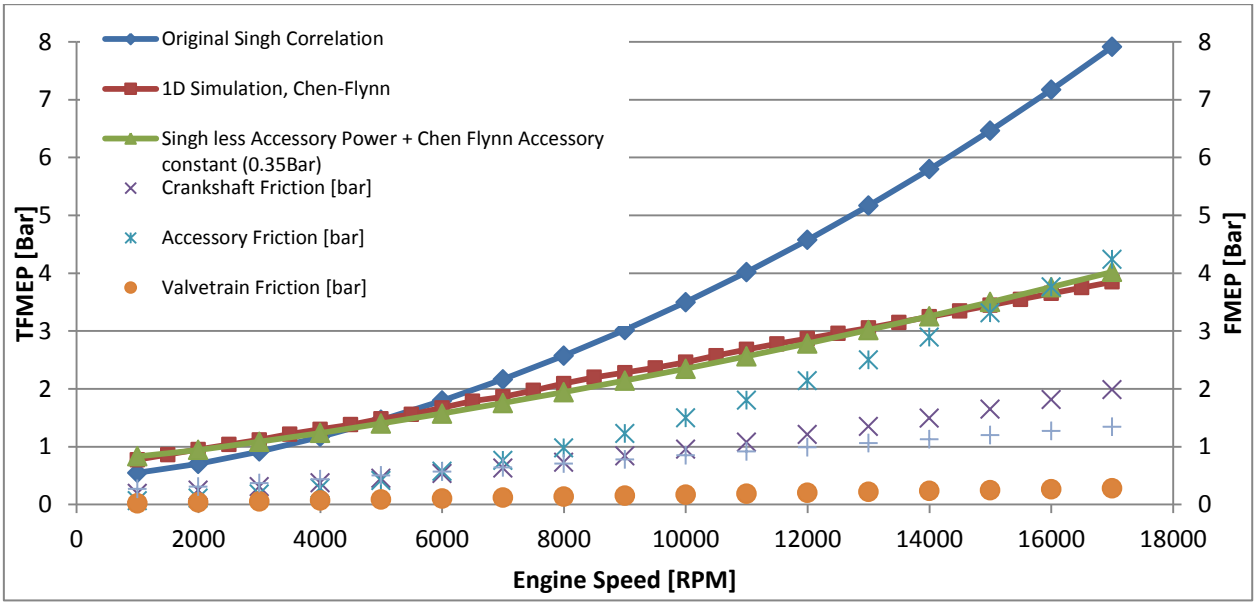

Figure 13: *The graph of TFMEP [Bar] against Engine Speed [RPM]*

Table 8: *The geometrical components used in Singh's correlation.*

Bore [mm]		81
Stroke [mm]		48.5
D_b [mm]	Bearing Diameter	38
L_b [mm]	Length of Bearing	40
n_c	Number of Cylinders	1
n_b	Number of Bearings	2
L_v [m]	Maximum Valve Lift	10
n_v	Number of Valves	4
V_d [m^3]	Displacement Volume	250000
k [kN/m]	Stiffness	12.84
L_s [mm]	Skirt Length	40
r_c	Compression Ratio	12
K	Constant	1.3
P_i [kPa]	Intake Pressure	100
P_a [kPa]	Atmospheric Pressure	100

Valvetrain Design and Manufacture:

Valve train design on a naturally aspirated Kawasaki ZX6R is currently being carried out by one of the team members. The motivation to design new camshafts is to reduce fresh air from going straight through the engine of the turbocharged engine. The effects of scavenging at high engine speeds created by large valve overlap are now undesired in the turbocharged engine thus the need to redesign new camshafts.

A separate simulation package, Ricardo VALDYN, was used to design and model the performance of the new cam profiles. As seen in the Figure 14 the acceleration at 15,000rpm, the agreed maximum engine speed for this engine, is within acceptable limits with no evidence of valve bounce being present. From the acceleration plots, the velocity and displacement curves were derived and plot as shown in Figure 14. A custom test rig was designed and built to test for valve bounce. This test bench involves a Kawasaki ZX6R cylinder head complete with the tested camshaft, which are rotated by a variable frequency driven electric motor.

To convert the optimum lift curve given by Valdyn into a cam profile, a short program was written in C. For each lift point at a one degree interval crank angle, a set of equations were applied to

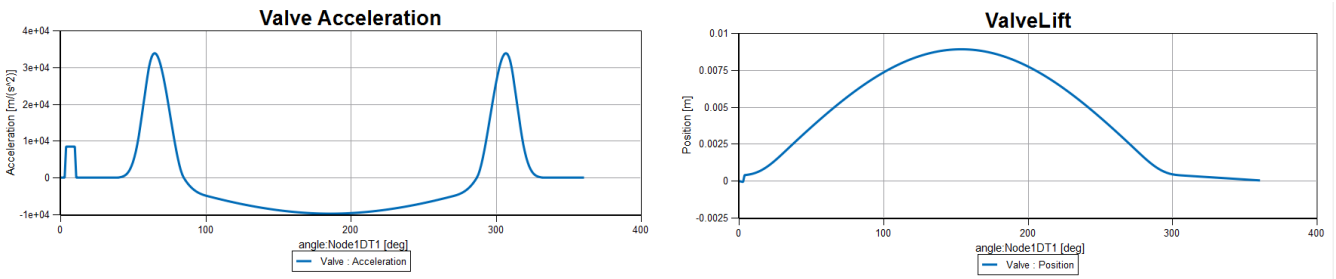

Figure 14: *The graph of Valve Acceleration and Valve Lift against Crank Angle [Deg]*

emulate the flat surface follower and generate the cam lobe from the valve lift.. These points would then be imported into AutoCad to draw the cam profile together with the complete camshaft as shown in Figure 14. A prototype camshaft has been designed and manufactured in this manner with a single lobe to test the new cam profile. The manufacturing of the camshaft was carried out on a CNC lathe. A CAD model was imported into OneCNC, a CAD/CAM software package which allows you to create toolpaths for a CNC Lathe. This package would then convert the toolpaths into G-code for the CNC controller. Some modifications to this G-code had to be done as it was not fully compatible with the Fanuc controller of the CNC lathe being used. Figure 14 shows the cam profile being manufactured using a horizontal milling tool. Further tests are being carried out on the test bench mentioned previously to validate the simulation and manufacturing processes. The next step towards manufacturing a complete camshaft with all the cam lobes is to manufacture a camshaft blank and heat treat it to achieve the required surface hardness. A cam copying machine would be used at a third-party engineering workshop which would copy the new profile machined using the CNC lathe and cut out these new profiles on the camshaft blank provided.

Figure 15: *The camshaft being manufactured on a 3-axis CNC lathe*

Modelling the air box and filter using co-simulation with Computational Fluid Dynamics (CFD).

Co-simulation with CFD Code, Ansys Fluent was used to model the air box volume. The co-simulation captures the effects of details in the air box that are otherwise not resolved.

The Empirical data gathered from **the air filter experiment** was used to define a porous media region in the space occupied by the air filter in the air box, Ansys documentation gives a procedure for determining the coefficients from experimental data. A second order polynomial was fitted to the plot of v vs. ΔP for the chosen air filter. Ansys Fluent models porous media by adding a momentum source term to the standard flow equations, consisting of a viscous loss term and an inertial loss term as given by the equation below:

$$S_i = -\left(\sum_{j=1}^{3} D_{ij}\mu v_j + \sum_{j=1}^{3} C_{ij}\frac{1}{2}\rho|v|v_j\right)$$

The thickness of the porous media was accounted for by the equation.

$$\Delta p = S_i \Delta n$$

The determined values were obtained from the K&N SU HS4 filter experimental flows were: 1.91e5 m^{-2} for the viscous resistance coefficient and 43m^{-1} for the inertial resistance in direction 1 and 3 orders of magnitude higher in directions 2 and 3. To avoid turbulence in the porous media region, the zone was constricted to laminar flow. Direction vector 1 was along the flow and 2 was in the plane of the disc filter.

A detailed model including a filter with corrugations, similar to the K&N and an airbox designed using best judgement and assuming a compact unit as desirable was designed using Ansys design modeller. However the coupled simulation was very slow and subsequently two simpler designs were generated and simulated. The models are shown in *Figure 16*. Mesh statistics for the three models are given in Table 9. This shows that there was more than an order of magnitude difference in the number of nodes between each model. The pressure drop coefficients were corrected for the areas and thickness.

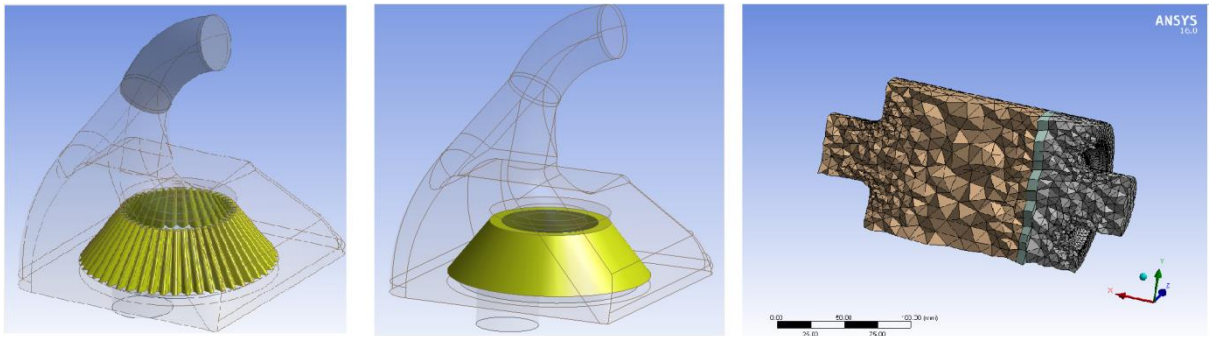

Figure 16: *Geomety Illustrations for the Filter and Air Box in Order of Complexity.*

Table 9: *Mesh Statistics*

	Nodes	Elements	Max Skew	Min OrthQuality	Tot.Vol
Corrugated Air Cleaner Detalied Airbox	2344520	13707475	0.93234	0.16069	1.2L
Conical Air Cleaner Detailed Airbox	136583	673916	0.86271	0.16797	1.2L
Disk Air Cleaner Simple Airbox	12507	63785	0.76432	0.33137	1.2L

The tutorial for co-simulation with Ansys Fluent was referenced for establishing a co-simulation method. The method was largely followed with few exceptions, since the species present in the air box are less than the species in an intake manifold with EGR. This allowed for more species to be ignored. In order to detect convergence and monitor results progress solution monitors for pressure and mass flow were used. Following the result from these monitors it was noted that the pressure history at the boundaries was increasing linearly when both boundaries were flow boundaries. Changing the downstream boundary to a pressure inlet resulted in the expected oscillatory response. It should be noted that co-simulation with Ricardo Wave-Fluent was actively being pursued for the last weeks as part of a Masters thesis by one of the authors of this report. However co-simulation could not be established. The success to co-simulate GT-Power with Fluent in the relatively short time span of the last days was due to the detailed tutorials provided in the documentation.

Due to time limitations only the 11,000RPM case was co-simulated. For the co-simulation 20 cycles in GT-Power without Fluent calls were simulated followed by 3 cycles with co-simulation. Figure 17 shows the pressure traces along the flow path were it could be noted that the highest pressure oscillations are in the exhaust port as expected, with diminishing amplitude further away from the engine. It was further noticed that the filter dampened the oscillations dramatically.

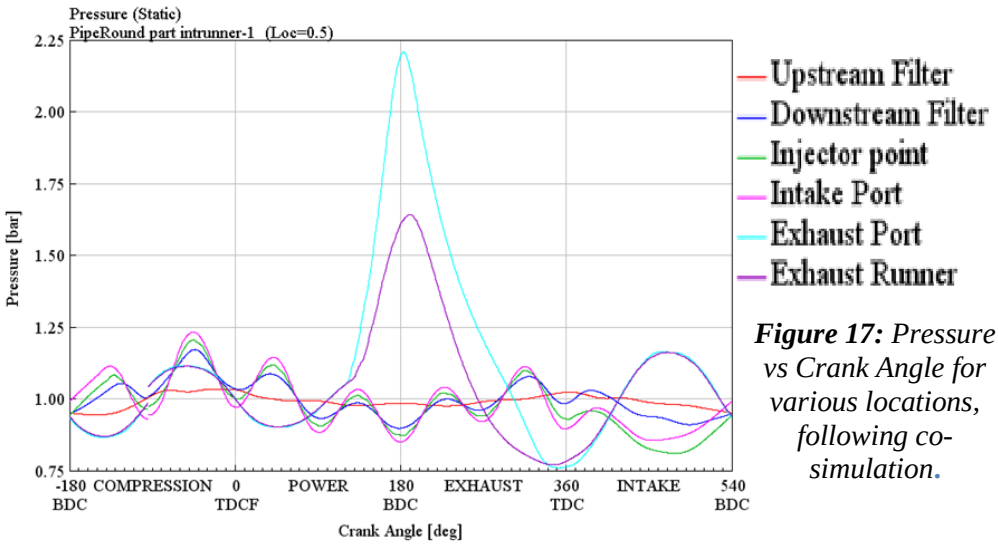

Figure 17: *Pressure vs Crank Angle for various locations, following co-simulation.*

Conclusion:

It was noted that the air filter and the airbox volume had the most impact on engine performance. On further analysis, from the response coefficients plot it was noted that the engine speed with intake duration was the second most influential factor on engine torque and power, which is expected since larger valve durations at higher engine speeds is essential for sufficient scavenging. The Singh correlation gave the possibility to calculate the component frictions. However the total

friction from Singh was significantly higher than that from the Chen-Flynn. Since the auxiliary component is a function of speed in Singh, the constant Chen-Flynn auxiliary component was used instead resulting in extremely good fit.

The values below state the optimum values for the intake and exhaust parameters obtained from separate respective DOEs.

Intake Optimum Parameters		**Exhaust Optimum Parameters**	
Intrunlength	10mm	Exhrunlength	100mm
Intrundiameter	49mm	exhrundiameter	46mm
intportdiameter	38mm	exhportdiameter	43mm
intportlength	13mm	exhportlength	25mm
D_ASP	35mm	D_SCA	27mm
intdur	1.15	exhdur	1.2
intlift	1.1	exhlift	1.1
intvalveportlength	12mm	exhvalveportlength	2.4mm
Airbox Vol	1200000mm3		
D_Throttle	52mm		

Bibliography

[1] M. Farrugia, "MEC4011 WAVE Assignment," [Online]. Available: http://staff.um.edu.mt/mario.a.farrugia/WaveAssignment.pdf. [Accessed 2017 04 30].

[2] R. W. Fox and A. T. McDonald, "Internal Incompressible Viscous Flow," in *Introduction to Fluid Mechanics*, Indiana, Wiley, 1998, pp. 351-354.

[3] M. Farrugia, "FSAE: Engine Simulation with WAVE," 11 05 2004. [Online]. Available: https://www.ricardo.com/Documents/Downloads/pdf/wave_engine_simulation_wave.pdf. [Accessed 30 04 2017].

[4] H. Hamid and M. Ashraf Ali, "Octane Blending," in *Handbook of MTBE and other Gasoline Oxygenates*, New York, Marcel Dekker, 2004.

[5] J. P. Azzopardi, "Analysis of Engine Downsizing: An Experimental Investigation of Incylinder Pressure and Knock," University of Malta, Msida, 2014.

[6] N. Grech, "SI Turbocharging Simulation and Fuel Injection Implementation," Univ. of Malta, Msida, 2007.

[7] G. Sammut and A. C. Alkidas, "Relative Contributions of Intake and Exhaust Tuning on SI Engine Breathing - A Comuputational Study," *SAE Technical Papers 2007-01-0492,* 2007.

[8] A. Singh, "A friction prediction model for small SI engines," Missouri University of Science and Technology, 2013.

[9] E. Pipitone, "A New Simple Friction Model for S.I. Engine," *SAE Paper 2009-01-1984,* 2009.

[10] J. B. Heywood, "Engine Friction and Lubrication," in *Internal Combustion Engine Fundamentals*, McGraw-Hill Education, 1988, pp. 712 - 745.

[11] "Engineering Toolbox," [Online]. Available: http://www.engineeringtoolbox.com/pitot-tubes-d_612.html. [Accessed 30 04 2017].

30th April 2017

Adrian Camilleri, Carl Caruana, Jean-Paul Farrugia, Supervised by: Dr. Mario Farrugia